Surface & Coatings Technology 244 (2014) 117–122

Contents lists available at ScienceDirect

Surface & Coatings Technology

journal homepage: www.elsevier.com/locate/surfcoat

Numerical study on interfacial delamination of thermal barrier coatings with multiple separations

Xueling Fan [a,b], Wei Jiang [c], Jianguo Li [a], Tao Suo [c], T.J. Wang [a,*], Rong Xu [a]

[a] State Key Laboratory for Strength and Vibration of Mechanical Structures, School of Aerospace Engineering, Xi'an Jiaotong University, Xi'an 710049, China
[b] Department of Mechanical Engineering, Faculty of Science and Technology, Tokyo University of Science, Chiba 278-8510, Japan
[c] School of Aeronautics, Northwestern Polytechnical University, Xi'an 710072, China

ARTICLE INFO

Article history:
Received 10 October 2013
Accepted in revised form 24 January 2014
Available online 10 February 2014

Keywords:
Delamination
Separation
Coalescence
Degradation
Thermal barrier coatings
Energy release rate

ABSTRACT

Coating film generally fails by spalling on cooling after prolonged thermal cycling. Cross-section SEM images show that numerous separations exist at the coating–substrate interface even in the as-processed condition. Upon cooling from the high deposition temperature to room temperature, the difference in the thermal expansion coefficients between the substrate and the coating film makes these multiple isolated separations grow, coalescence and linking up, and, finally leads to coating buckling upon a critical size. In this paper, the interfacial degradation of thermal barrier coatings with multiple separations is investigated by combining the virtual crack closure technique with the user element subroutine "UEL" of Abaqus. The effects of interfacial separation morphology on the energy release rate (ERR) are quantified. Results show that the propagation and coalescence of local separations will dramatically alter the load capacity of the studied structures. It revealed that the larger the initially bonded zone is, the larger the steady ERR value is and the later the local maximum ERR value appears. It is believed that the concerted modeling technique will greatly benefit the understanding of the mechanics associated with the linking-up of subcritical flaws to form a critical flaw size for buckling.

1. Introduction

Film–substrate structures have been used over a wide range of applications including stretchable electronic device, thermal barrier coatings (TBCs) and so on [1–5]. The mechanical behavior of brittle coating or film plays an important role in understanding the response of coating as either cohesive fracture or interfacial delamination [6–8]. Through–thickness surface cracks relieve stresses in the coating, when they are running from the coating surface to the underlying layer. So through–thickness surface cracks have a positive potential in reducing effective modulus of elasticity and improving the thermal cyclic durability of coatings without affecting the thermal conductivity [9–14]. The horizontal delamination cracks, on the other hand, may reduce the thermal shock resistance and durability of the film substrate structures [15–20]. Based on experimental results, the large residual stresses accumulated in thermal cycling is the key factor to the formation of local interfacial separations. Finally, the large residual stresses may lead to spallation failure of the coating [6,17]. More recently, research focus on the competitive mechanisms between surface cracks and interfacial delamination [21–26]. Kokini et al. [21,22] and Wu et al. [23] analyzed the interfacial delamination mechanisms in TBCs with multiple surface cracks. As shown in a previous work by Mei et al. [24], the triggering and restraining of interfacial delamination depend on the material mismatch and interface toughness. They proposed a failure map to distinguish the failure behavior of film–substrate with different material mismatch. Fan et al. [25,26] examined the effect of surface cracks on the initiation and propagation of delamination in TBCs. The results shown that, as surface crack spacing increases to a critical value, horizontal delamination cracks will be triggered in case of relatively weak adhesion. They stated that an appropriately surface crack density, which can be achieved by controlling the deposition parameters, helps to enhance the durability of TBCs.

Until recently, the propagation of a single interface crack is adopted to numerically study the TBCs failure. However, micro–structural analysis reveals that the roughening (rumpling) of bond coat leads to the nucleation, progressive growth, and accumulation of separated regions (Fig. 1), and eventually, spallation failure of the TBCs [27–30], which is hard to be simulated by the propagation of a single crack. From a manufacturing, as well as materials selection perspective, clarifying mechanisms of failure and being able to predict life remains an essential and core task in optimizing the coating system. To clarify the failure mechanisms, eventually, it is essential to concern linking up of sub–critical flaws in TBCs and formation of a critical size flaw leading to the buckling of the TBCs. This process determines the thermal cycle life of TBCs and makes an important contribution for life prediction models, but it has not really been analyzed.

The emphasis of this work is on the modeling of typical interfacial degradation mechanism of TBCs, including growth, coalescence and linking up of multiple local separations between the coating film and

* Corresponding author. Tel.: +86 29 82663318; fax: +86 29 82669044.
E-mail address: wangtj@mail.xjtu.edu.cn (T.J. Wang).

0257-8972/$ – see front matter © 2014 Elsevier B.V. All rights reserved.
http://dx.doi.org/10.1016/j.surfcoat.2014.01.045

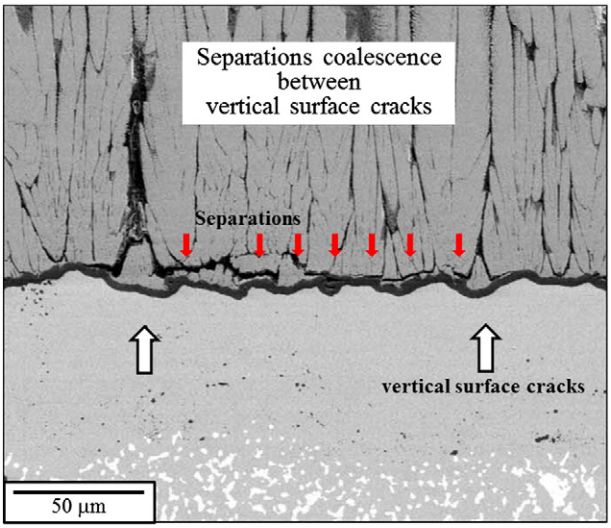

Fig. 1. Typical cross–section microstructure showing surface cracks with multiple separations at the interface [30].

the bond coat. Section 2 introduces the numerical technique to modeling thin film–substrate structure with multiple interfacial separations. In Section 3, we talk about the fracture driving force for the interfacial delamination with multiple separations at the interface. And we analyze influences of separation size and bonding ratio. In Section 4 we summarize the findings and emphasize the importance of the concerned modeling technique for the understanding of the failure mechanics of multilayer structures.

2. TBCs with multiple interfacial separations

2.1. Statement of the problem

TBCs mainly comprise thermally insulating ceramic materials, such as yttria–stabilized zirconia (YSZ), deposited onto the structural loads sustain superalloy substrate. To provide the oxidation protection, a layer aluminum–containing bond coat exits between the substrate and coating film. Under typical operating conditions, a thermally grown oxide (TGO), typically alumina of several micrometer thickness forms between the bond coat and the ceramic top coat. Several factors such as the thermal–expansion mismatch stresses, the oxidation of the metal, the variation of microstructures and the degradation of interfacial govern the failure mechanisms of TBCs. As stated above, small isolated local separation nucleates, grows, linking up, coalescence, and buckling until failure occurs by spallation. That means that any practical numerical model should consider the exist of multiple isolated separations at the interface. To simplify the problem, the curvature of the interface is ignored. As a result, a two–dimensional plane strain model is constructed, as show in Fig. 2, where h_f is the film thickness, L_b and L_d are the lengths of bonding and the debonding portions of the interface, respectively.

2.2. Fracture mechanics of interface element

Fracture mechanics approach is often adopted to simulate crack propagation, in which the crack driving force, characterized by energy release rate (ERR) or stress intensity factor (SIF), is computed and compared to the corresponding fracture toughness. Various models and methods have been proposed to fulfill different requirements of engineering problems. The virtual crack closure technique (VCCT), firstly proposed by Rybicki and Kanninen [31] and extended by Shivakumar et al. [32], is one of the most popular and powerful tools to obtain crack driving force. In this paper, the modeling technique for interfacial

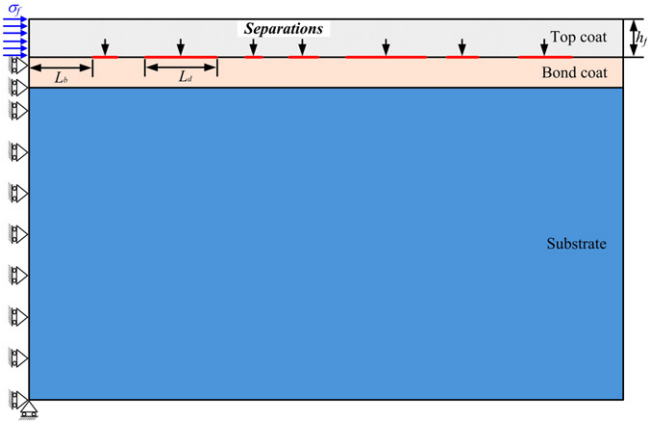

Fig. 2. Schematic illustration of two–dimensional plane strain model for thermal barrier coatings (TBCs) with local isolated separations at the interface between bond coat and top coat.

degradation analysis with multiple separations at the interface is based on the idea of Xie and Biggers [33,34]. An interface element was constructed to calculate the ERR based on the VCCT in conjunction with finite element analysis. Then, the element was implemented into commercial software and was proved to be simple, efficient and robust in crack growth problems.

Fig. 3 shows the definition of interface element, in which a very stiff spring is placed between the node pair at the crack tip (N1 and N2) to calculate the internal forces, while the node pair immediately behind the crack tip (N3 and N4) is used to extract information for displacement openings. Moreover, the node ahead of the crack tip (N5) is introduced to define the crack growth direction and length. Particularly, the top set nodes of the interface elements coincide with their corresponding lower sets before fracture happens. For clarity, the distance between the top node set and the bottom node set has been greatly exaggerated in Fig. 3.

According to Irwin's crack closure integral method, the work required to extend a crack by an infinitesimal distance is equal to the work required to close the crack to its original length. Thus, the ERR components can be expressed as

$$G_I = \lim_{\Delta\to 0}\frac{1}{2\Delta}\int_0^{\Delta}\sigma_{yy}(\Delta-r)\delta_y(r)dr \tag{1}$$

$$G_{II} = \lim_{\Delta\to 0}\frac{1}{2\Delta}\int_0^{\Delta}\sigma_{xy}(\Delta-r)\delta_x(r)dr \tag{2}$$

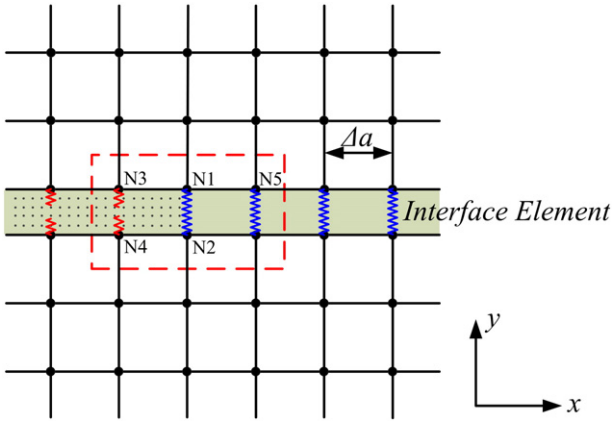

Fig. 3. Virtual crack closure technique based interface element for four–node element (note that the thickness of interface element is exaggerated for clarity).

$$G = G_I + G_{II} = \lim_{\Delta\to 0}\frac{1}{2\Delta}\int_0^{\Delta}\left[\sigma_{yy}(\Delta-r)\delta_y(r) + \sigma_{xy}(\Delta-r)\delta_x(r)\right]dr \quad (3)$$

where Δ is a small crack extension; σ_{yy} and σ_{xy} are the normal and shear tractions, respectively, at a distance r ahead of the crack tip; and δ_x and δ_y are the displacement components along the x (sliding mode) and y (opening mode) axis, respectively.

It is proved by Rybicki and Kanninen [31] that the integrals in Eqs. (1) and (2) can be computed numerically by finite element analysis using VCCT. For the four–node rectangular element as shown in Fig. 3, we can recast the equations to calculate the ERR components at the crack tip nodes of Eqs. (1) and (2) to capture the discrete nature of finite element analysis, and yields

$$G_I = \frac{F_y\Delta v}{2B\Delta a} = \frac{F_y(v_3-v_4)}{2B\Delta a} \quad (4)$$

$$G_{II} = \frac{F_x\Delta u}{2B\Delta a} = \frac{F_x(u_3-u_4)}{2B\Delta a} \quad (5)$$

where Δa is the length of the element ahead of the crack tip (defined by N5 and N1), and F_x and F_y are the shear and opening forces at the crack tip (at nodal points N1 and N2), u_i and v_i are the shear and opening nodal displacement components along x and y axes, respectively. The new created crack surface is calculated as $\Delta a \times B$, where it is assumed that the two–dimensional model is of unit thickness, that is $B = 1$.

Then, the total ERR can be calculated from the individual mode components as

$$G = G_I + G_{II}. \quad (6)$$

The VCCT proposed by Rybicki and Kanninen [31] does not make any assumptions about the forms of the stresses and displacements. Therefore, the method can be used with non–singular, linear, finite element simulation to get accurate ERR values.

To model the debonding of interface, the following general form fracture criterion can be selected to determine the initiation and propagation of crack

$$f = \left(\frac{G_I}{G_{IC}}\right)^{\alpha} + \left(\frac{G_{II}}{G_{IIC}}\right)^{\beta} \geq 1 \quad (7)$$

where f is the crack growth parameter, crack will grow when f is greater than or equal to one, and G_{IC} and G_{IIC} are the critical values (fracture toughness) corresponding to mode I and mode II fracture, respectively, which are assumed to be constant and should be determined experimentally.

For the studied four–node two dimensional element, the interface element has five nodes, N1, N2, N3, N4, and N5. Therefore, its displacement array can be characterized by $\{U_1, U_2, U_3, U_4, U_5, U_6, U_7, U_8, U_9, U_{10}\}$. Assume the stiffness components of the spring allocated between node pair N1 and N2 are K_x and K_y, then the nodal forces at the crack tip can be calculated as

$$F_x = K_x(U_1-U_3),\ F_y = K_y(U_2-U_4) \quad (8)$$

and the shear and opening nodal displacement components behind the crack tip are

$$\Delta u = U_5-U_7,\ \ \Delta v = U_6-U_8. \quad (9)$$

The crack growth direction is defined by node N5 and node N1, while the crack growth length equals to the distance between N5 and N1 along x-axis, that is

$$\Delta a = |x_5-x_1|. \quad (10)$$

Substituting Eqs. (8) to (10) into Eqs. (1) to (3), we can immediately get the ERR values.

Therefore, with this interface element, ERR values can be output simply as finite element analysis is performed since the node force and displacement are basic information of any finite element method. Furthermore, with the implementation of fracture criteria, crack growth can be also directly analyzed with a fracture mechanics approach. Particularly, once the fracture parameter f is greater than or equals to one, the crack grows and the stiffness matrix of the interface element is set to zero.

2.3. Numerical modeling of TBCs with isolated separations

To evaluate the interfacial degradation of TBCs, the interface element introduced in Section 2.2 is implemented into commercial finite element analysis software ABAQUS with UEL. Numerical calculations are carried out by using the commercial finite element code ABAQUS. The TBCs structure is assumed to be sufficiently thick compared to its in–plane geometry such that the problem can be approximated by a two–dimensional plane–strain model. An array of interface elements, which characterizes the bonded area, is randomly spaced at the interface between bond coat and top coat. Symmetry of the problem allows apply symmetrical constraints on the left edges of substrate and bond coat layers. Considering the actual distribution of thermal stress in coating, uniform normal traction is assumed to acting onto the surface of the vertical crack (Fig. 2). For a typical finite element model of the tri–layer TBCs structure, non–uniform mesh is adopted with fine mesh modeled around the interface. Indeed, to verify the numerical reliability of the solutions for the problem studied, the convergence of mesh configuration and characteristic distance should be checked carefully. All the three layers are treated as isotropic and elastic materials. Their mechanical properties and geometry parameters are listed in Table 1. The reported delamination toughness of TBCs varies from 10 to 100 J/m^2 [36]. In this paper, 20 J/m^2 is chosen as the critical ERR value. The thicknesses of the top coat and bond coat are selected to be 200 μm and 100 μm, respectively. Infinite elements are used for the substrate to eliminate possible constraint effects of the underlying layer.

3. Results

3.1. On local separation size effect

In this section, the influence of local separation size on the interfacial delamination emanated from the root of surface crack is firstly examined. Fig. 4 depicts the relationship between the force and displacement at the loaded points for different separation sizes L_d as well as the defect–free case.

The basic outcome of the force–displacement curve is that the initiation of delamination from the root of surface crack requires to increase the load until reaching a local maximum value. And then, it propagates and coalesces with separation ahead, which leads to a suddenly loss in load carrying capacity. To clearly indicate this kind of fracture behavior, a main interface crack is defined which originates from the root of surface crack. Recall that uniform normal traction is applied onto the surface of vertical crack with a symmetry boundary

Table 1
The mechanical properties and geometry parameters for top coat, bond coat and substrate (after Ref. [35]).

	Elasticity modulus (GPa)	Poisson ratio	Thickness (μm)
APS 8YSZ coating	45	0.1	200
NiCoCrAlY bond coat	186	0.3	100
Superalloy substrate	200	0.3	Infinite

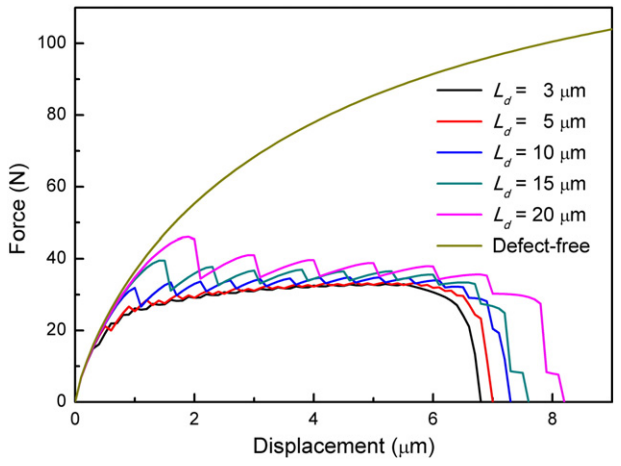

Fig. 4. Force vs. displacement at the loading points for different separation sizes L_d (results obtained for the bonding ratio of 50%).

condition applying for the bond coat and substrate. The interfacial crack will grow incrementally toward the adjacent debond zone, from left to right along the interface, until it fractures all the interface elements in the first bonded area L_b. Then, it coalesces with the adjacent separation of size L_d, which corresponding to the first drop in the traction–separation curve. Now, the crack length becomes $L_b + L_d$ and it grows toward the second bonded area until it run into the second separation. Now the crack has updated its length to be $2L_b + L_d$, which corresponding to the second drop in the traction–separation curve. After coalescences with the second separation, the crack has a new length of $2L_b + 2L_d$. Keep following this process, we can get the entire deformation history show in Fig. 4.

An important feature of Fig. 4 is that due to the enlarging of initially bonded area increasing values of maximum force is obtained. It does not come as a surprise though, since the strain energy stored in the coating for a larger initially bonded area is higher than those of smaller initially bonded area. Thus, the fracture of a larger bonded zone needs more work applied, which leads to the higher local maximum value. In this case, the cohesive energy required to fail the interface, i.e. the area under the traction–separation curve is also higher. In comparison, in case of smaller initially bonded area, edge delamination is easily be triggered, which is characterized by the earlier appeared local maximum force in the curve.

The predicted normalized ERR as a function of the normalized interfacial delamination length is shown in Fig. 5(a) and (b) for different separation sizes. In this work, the ERR is normalized by $\sigma_f^2 h_f / \overline{E}_f$, where σ_f is the stress in the coating film, h_f is the coating thickness, and $\overline{E}_f = E_f / \left(1 - v_f^2\right)$ is the plane strain modulus of the coating with Young's modulus E_f and Poisson's ratio v. The separation size and the crack length are normalized by the coating thickness h_f. Note that the gaps in the curves is caused by the successive defects at the interface. Herein, the ERR values are calculated by the node force at the moment crack tip approaching to its left adjacent node. At the moment, the crack driving force equals to the stored energy in the film coating.

It is seen that as the normalized separation size decreases the local maximum ERR decreases remarkably. For the two compared cases, there is a decrease to half in the ERR values when the normalized separation size L_d / h_f changes from 0.1 to 0.05. Obviously, in case of large block size (defined by $L_b + L_d$) additional energy is accumulated in the coating before crack grows to the next defect, which means in this case it is more difficult to break down the bonded area and coalescence with the adjacent local separations. From Fig. 4 we can find that for a larger initially bonded area, the curve drops down later and a higher node force value is reached. As a result, the energy stored, area under the curve, is higher than that of smaller initially bonded area, which

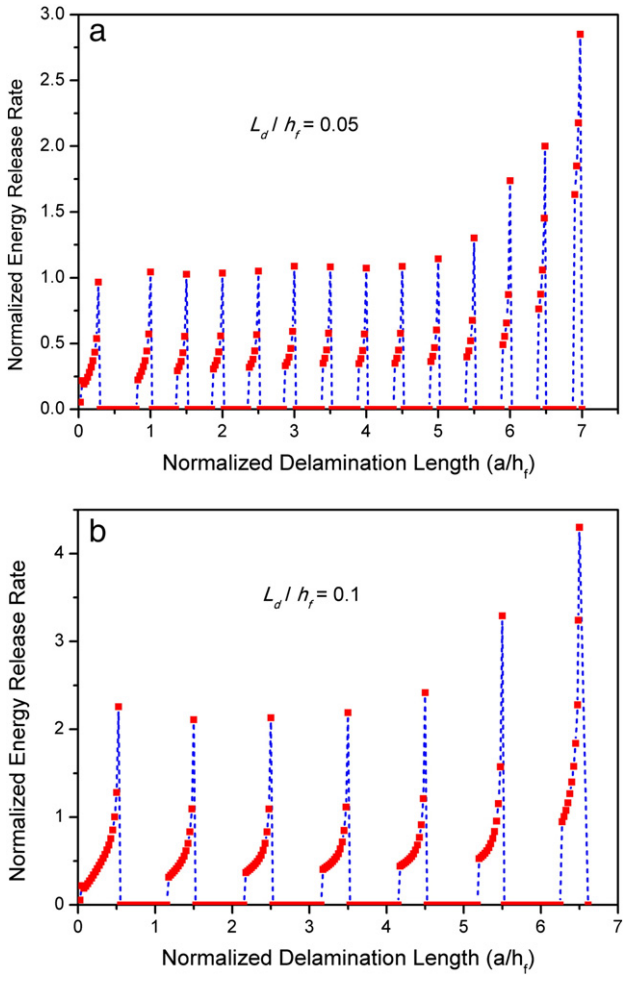

Fig. 5. Evolution of normalized energy release rate (ERR) $\overline{G}$ considering coalescence with local separations at the interface between top coat and bond coat: (a) $L_d / h_f = 0.05$; (b) $L_d / h_f = 0.1$ (here ERR is normalized by $\sigma_f^2 h_f / \overline{E}_f$).

helps to explain the results presented in Fig. 5. According to the energetic condition, which states that crack growth occurs once the energy stored exceeds the fracture energy needed for delamination at the interface, we conclude that the edge delamination can be easily formed for smaller initially bonded area. The results coincide with those provided by Wright and Evans [37] that final failure of TBCs occurs by edge delamination whenever the mode II toughness of the interface, which is set to be a relatively smaller value of 20 J/m^2 in this work, is lower than the indicated value and falls into an edge delamination dominant domain. The results suggested that in case of relative small initially bonded area at the root of surface crack the key point is to avoid edge delamination. However, in case of relatively high mode II interface toughness more attention should be paid on the quantitative characterizing the largest separation size, which facilitates and accelerates the TBCs failure in a noteworthy way [30]. Further investigation should be conducted to analyze the buckling drive TBCs spalling. As delamination propagates, the effects of mode I become significant, especially it will dominate the fracture mechanisms as it approaches to right edge of the model. As a result, due to the finite–width of the tested specimen the crack driving force ramps up instead of maintains a relative constant value.

3.2. On bonding ratio effect

Fig. 6 shows the influence of bonding ratio on the crack driving force of the interfacial delamination, where the bonding ratio is defined by

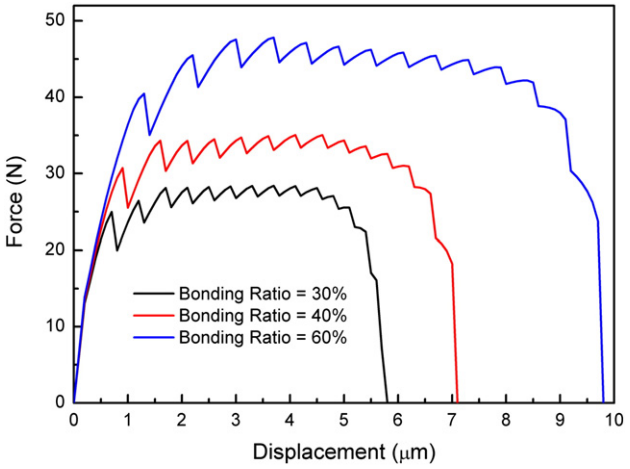

Fig. 6. Force vs. displacement at the loading points for different bonding ratios (herein, bonding ratio is defined by $L_b / (L_b + L_d)$).

the ratio of bonded length L_b to one block size $L_b + L_d$. The influence of bonding ratio on the ERR values is similar to that of defect size. The coalescence of the delamination with local separations is characterized by the successive drops in the force displacement curve. It is observed that due to the increasing of bonding ratio maximum force keeps increasing. In case of lower bonding ratio, less energy is required to break down interface elements. So the loading curve lies under that of higher bonding ratio and drops down earlier. Moreover, the difference between the minimum and the maximum ERR values within one block is relatively small for lower bonding ratio, which makes the force–displacement curve more smooth.

Fig. 7 plots the evolution of normalized ERR values with the propagation of interfacial delamination for different bonding ratios. As discussed in the previous section, more interface elements increase the fracture resistance by requiring additional energy for the growth of delamination. As a result, the larger the initially bonded area is, the larger the steady ERR value is and the later the local maximum ERR value appears. Since edge delamination can be easily trigged for smaller initially bonded area, in this case, the bonding strength should be enhanced to avoid edge delamination especially when a large separation exists at the interface.

It should be noted that before the main interface crack arrives to adjacent separations some interface elements already broken down in the nearby bonded area. It is clearly illustrated in Fig. 7a. The main interface crack is expected to coalescence with six interface elements for each block $(L_b + L_d)$. However, local separation growth already happens in the adjacent bonded zone, which means several interface elements have been fractured. For example, when the normalized delamination length is about 5, local separation has propagated and coalescenced with three interface elements. As a result, only tree numerical data points are provided, which corresponds to the three still bonded interface elements. This partially coalescence of separations is important when local imperfections exist. Buckling can be easily triggered and should be taken into account accordingly in this situation.

Another feature of Fig. 7 is that for a given defect size, the local maximum ERR keeps constant as the interface crack propagates. This is reasonable since the bonded area and the local separations are assumed to be uniformly distributed and without imperfections, which means same amount of energy is required to break down each interface element.

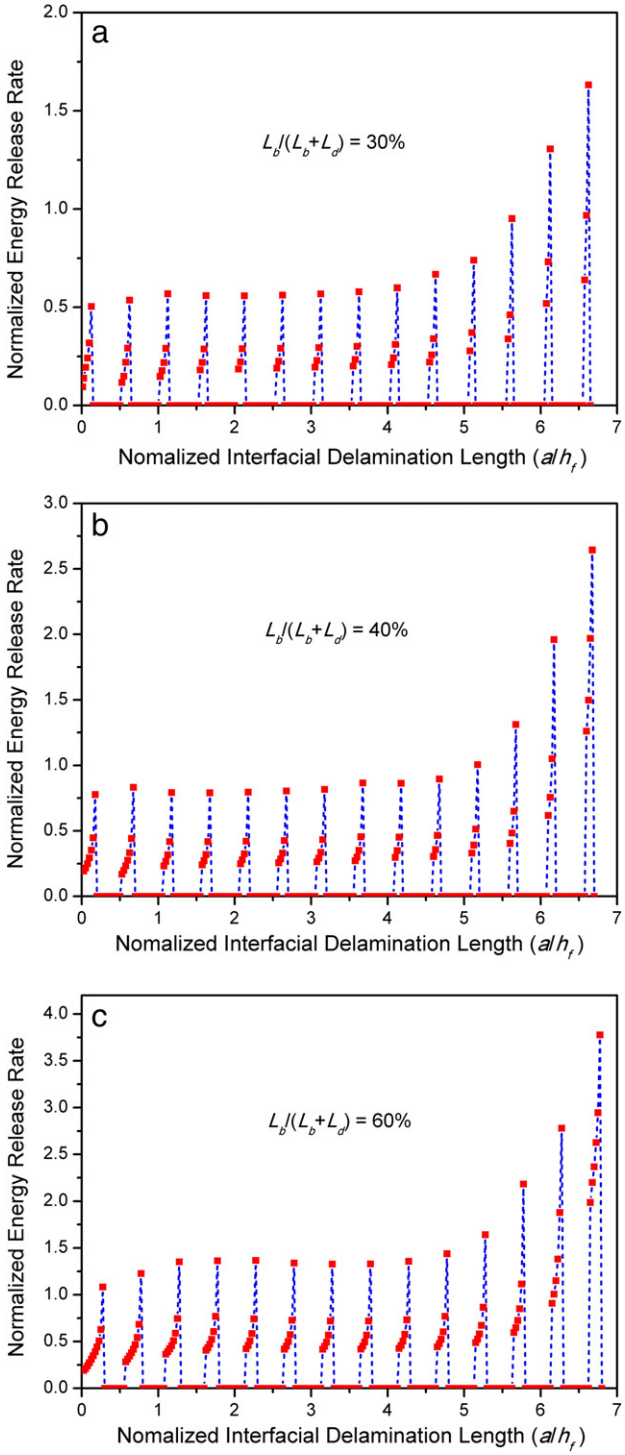

Fig. 7. Evolution of normalized ERR as a function of interfacial delamination length: (a) $L_b / L = 0.3$; (b) $L_b / L = 0.4$; (b) $L_b / L = 0.6$, where $L = L_b + L_d = 20$ μm.

4. Concluding remarks

This paper describes the interfacial delamination of thermal barrier coatings (TBCs) by using a virtual crack closure technique (VCCT) based interface element method. In this method, discrete user defined elements are placed between interfacial node pairs to model cohesive behaviors of adjacent surfaces. A major advantage of this "point–wise" discrete modeling approach is the capability to consider the effects of the growth, coalescence and linking up of local separations at the interface. This method can greatly facilitate the numerical simulation of interfacial degradation caused by an accumulation of damage from multiple isolated defects in thin film structures.

Depend on the deposition parameters, the mechanical properties of TBCs can change significantly with the coating microstructure. In practical, a wide variation in coating microstructure results in a large scatter

in system reliability, durability, and predictability. In this paper, the effects of separations size and bonding ratio on the interfacial delamination initiated from the root of surface cracks are further examined by implementing the interface element into commercial finite element software ABAQUS with user subroutine UEL. It reveals that the larger the initially bonded area is the larger the steady–state energy release rate value is and the later the peak value appears. Because larger initially bonded area at the root of surface crack increases the fracture resistance by requiring additional energy for delamination growth, which helps to postpone the formation of edge delamination.

The objective of this study is to evaluate the interfacial delamination of TBCs with multiple interface separations located at the crack path. This work is essential to concern linking up of sub–critical flaws in TBCs to form a critical size flaw for buckling. However, the key process of coating spalling failure has been proved to be more complex comprising of not only growth and coalescence of local separations but also its subsequent eventually buckling and spalling of whole coating from substrate. These aspects have not really been analyzed and should be addressed in future.

Acknowledgment

This work is supported by the State 973 Program of China (2013CB035700) the National Natural Science Foundation of China (11272259, 11321062 and 11002104) and Research Fund of Tokyo University of Science, Japan.

References

[1] C.D. Dimitrakopoulos, P.R.L. Malenfant, Adv. Mater. 14 (2002) 99–117.
[2] C. Keplinger, J.Y. Sun, C.C. Foo, P. Rothemund, G.M. Whitesides, Z. Suo, Science 341 (2013) 984–987.
[3] X. Feng, B.D. Yang, Y.M. Liu, Y. Wang, C. Dagdeviren, Z.J. Liu, A. Carlson, J.Y. Li, Y. Huang, J.A. Rogers, ACS Nano 5 (2011) 3326–3332.
[4] D.R. Clarke, M. Oechsner, N.P. Padture, MRS Bull. 37 (2012) 891–898.
[5] K. Zhou, M.S. Wu, Acta Mater. 211 (2010) 271–292.
[6] A.G. Evans, J.W. Hutchinson, Surf. Coat. Technol. 201 (2007) 7905–7916.
[7] R. Vaßen, A. Stuke, D. Stöver, J. Therm. Spray Technol. 18 (2009) 181–186.
[8] K. Zhou, L.M. Keer, Q.J. Wang, D.Y. Hua, Wear 271 (2011) 1203–1206.
[9] B.D. Choules, K. Kokini, T.A. Taylor, Mater. Sci. Eng. A 299 (2001) 296–304.
[10] A.A. Rizk, Int. J. Solids Struct. 41 (2004) 4685–4696.
[11] M.D. Thouless, Z. Li, N.J. Douville, S. Takayama, J. Mech. Phys. Solids 59 (2011) 1927–1937.
[12] X.L. Fan, W.X. Zhang, T.J. Wang, G.W. Liu, J.H. Zhang, Appl. Surf. Sci. 257 (2011) 6718–6724.
[13] W.X. Zhang, X.L. Fan, T.J. Wang, Appl. Surf. Sci. 258 (2011) 811–817.
[14] X.L. Fan, W.X. Zhang, T.J. Wang, Q. Sun, Surf. Coat. Technol. 208 (2012) 7–13.
[15] W.G. Mao, C.Y. Dai, L. Yang, Q.X. Liu, Y.C. Zhou, Int. J. Fract. 151 (2008) 107–120.
[16] W.G. Mao, C.Y. Dai, Y.C. Zhou, Q.X. Liu, Surf. Coat. Technol. 201 (2007) 6217–6227.
[17] Z.X. Chen, K. Zhou, X.H. Lu, Y.C. Lam, Acta Mater. 225 (2014) 431–452.
[18] T.Q. Lu, W.X. Zhang, T.J. Wang, Int. J. Eng. Sci. 49 (2011) 967–975.
[19] C.J. Li, Y. Li, G.J. Yang, C.X. Li, J. Therm. Spray Technol. 22 (2013) 1374–1382.
[20] R. Xu, X.L. Fan, W.X. Zhang, Y. Song, T.J. Wang, Mater. Des. 47 (2013) 566–574.
[21] S. Rangaraj, K. Kokini, J. Appl. Mech.-Trans. ASME 70 (2003) 234–245.
[22] B. Zhou, K. Kokini, Acta Mater. 52 (2004) 4189–4197.
[23] C.W. Wu, G.N. Chen, K. Zhang, G.X. Luo, N.G. Liang, Surf. Coat. Technol. 201 (2006) 287–291.
[24] H.X. Mei, Y.Y. Pan, R. Huang, Int. J. Fract. 148 (2007) 331–342.
[25] X.L. Fan, R. Xu, W.X. Zhang, T.J. Wang, Appl. Surf. Sci. 258 (2012) 9816–9823.
[26] X.L. Fan, R. Xu, W.X. Zhang, T.J. Wang, M. Kikuchi, The 9th International Conference on Fracture & Strength of Solids (FEOFS), 9–13 June, Jeju Island, Korea, 2013.
[27] V.K. Tolpygo, D.R. Clarke, Surf. Coat. Technol. 163–164 (2003) 81–86.
[28] V.K. Tolpygoa, D.R. Clarkea, K.S. Murphyb, Surf. Coat. Technol. 188–189 (2004) 62–70.
[29] B. Heeg, D.R. Clarke, Surf. Coat. Technol. 200 (2005) 1298–1302.
[30] B. Heeg, V.K. Tolpygo, D.R. Clarke, J. Am. Ceram. Soc. 94 (2011) S112–S119.
[31] E.F. Rybicki, M.F. Kanninen, Eng. Fract. Mech. 9 (1977) 931–938.
[32] K.N. Shivakumar, P.W. Tan, J.C. Newman Jr., Int. J. Fract. 36 (1988) R43–R50.
[33] D. Xie, S.B. Biggers, Finite Elem. Anal. Des. 42 (2006) 977–984.
[34] D. Xie, S.B. Biggers, Eng. Fract. Mech. 73 (2006) 771–785.
[35] X.Q. Cao, R. Vassen, D. Stöver, J. Eur. Ceram. Soc. 24 (2004) 1–10.
[36] Y. Yamazaki, A. Schmidt, A. Scholz, Surf. Coat. Technol. 201 (2006) 744–754.
[37] P.K. Wright, A.G. Evans, Curr. Opin. Solid State Mater. Sci. 4 (1999) 255–265.